ACS APPLIED MATERIALS & INTERFACES

Research Article

www.acsami.org

Growing Nickel Cobaltite Nanowires and Nanosheets on Carbon Cloth with Different Pseudocapacitive Performance

Huanwen Wang and Xuefeng Wang*

Department of Chemistry, Key Laboratory of Yangtze River Water Environment, Ministry of Education, Tongji University, Shanghai 200092, China

ABSTRACT: Controllable synthesis and high yield of functional nanomaterials on conductive substrates are highly desirable for energy conversion and storage applications. In this work, two different porous $NiCo_2O_4$ nanoarchitectures (including nanowires and nanosheets) are directly grown on carbon cloth collectors, which display a structure-dependence in their capacitive behaviors. Our results show that the nanowire morphology exhibits higher specific capacitance and better cycling performance in the three-electrode configuration. The pseudocapacitive difference is related to the surface area and pore structure of $NiCo_2O_4$ nanocrystals. This comparison among different morphologies reveals a process−structure−property relationship in electrochemical energy storage.

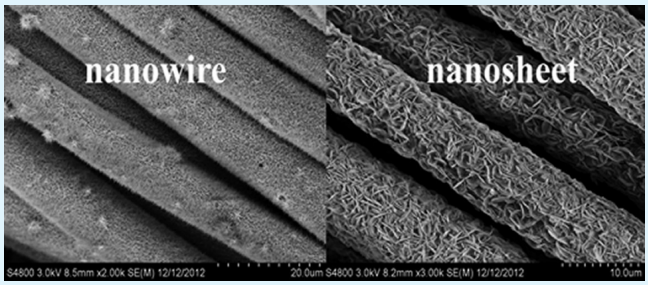

KEYWORDS: *$NiCo_2O_4$, carbon cloth, nanowires, nanosheets, capacitive behaviors*

1. INTRODUCTION

Compared to the single-component oxides, spinel cobaltites (MCo_2O_4; M = Mn, Ni, Zn, Cu, Mg, etc.) offer richer redox chemistry and combine the contributions from both Co and M ions.[1−3] For instance, through substitution of Mn for Co in the spinel Co_3O_4 lattice,[4,5] the oxygen reduction reaction activity of the catalyst could be obviously improved. Furthermore, $NiCo_2O_4$ has been reported to possess a much better conductivity, by at least 2 orders of magnitude, than those of NiO and Co_3O_4.[6] Lu and co-workers first showed supercapacitor application of the $NiCo_2O_4$ aerogel with largely enhanced capacitance.[7] Since then, there has been a variety of reports of the synthesis of different $NiCo_2O_4$ nanostructures for electrochemical energy storage. According to electrode structure, these works can be classified into two basic types: (i) binder-enriched and (ii) binder-free. In the former case, the $NiCo_2O_4$ powder is first fabricated by several techniques, including ball milling,[8] coprecipitation,[9−12] KIT-6 template,[13] hydrothermal,[2,6,14,15] and sol−gel.[7,16] Subsequently, the working electrode is prepared by the traditional slurry-coating technique for electrochemical measurement. Despite significant progress, the binder involved will greatly decrease the electrical conductivity of the electrode materials, hindering their potential application in supercapacitors. In the latter case, electroactive $NiCo_2O_4$ nanostructures are deposited on conductive substrates to be directly used as binder-free electrodes for supercapacitors. This electrode architecture avoids the use of other auxiliary components like conductive agents and binders to further optimize the electrode performance using a well-defined electrode network with minimum resistivity. Very recently, $NiCo_2O_4$ nanoneedle,[17] nanowire,[18] and nanosheets[19,20] have been grown on Ni foam collector, which shows ultrahigh specific capacitances. However, experimental evidence assumes that using nickel foam (even chemically etched) as current collector can bring about substantial errors to the specific capacitance values of electrode materials.[21−23] Gupta et al. demonstrated high rate charge−discharge capability by depositing $NiCo_2O_4$ film on stainless steel substrate;[24] however, the inflexible/rigid nature of stainless steel substrate prevents it from practical applications in harsh environments such as folding/twisting conditions.[25]

As a highly flexible and low-cost substrate, carbon cloth consisting of carbon fibers orienting in two directions shows some unique properties, such as high strength, high conductivity, and good corrosion resistance. These features render carbon cloth for application in field emission,[26] lithium-ion batteries,[27] dye-sensitized solar cells,[28] and photodetectors.[29] Considering the similar requisite characteristics of electrodes in optoelectronic devices and in supercapactiors, carbon cloth may be a promising current collector for conformal coating of transition metal oxides for supercapactiors without using any insulating binders.[30] In addition, one-dimensional (1D) and two-dimensional (2D) nanostructures have been intensely investigated as building blocks in electrochemical energy storage devices. However, to the best of our knowledge, there is still no report on the fabrication of 1D and 2D $NiCo_2O_4$ nanocrystals on carbon cloth for supercapacitors.

In this paper, we report the synthesis of nanostructured $NiCo_2O_4$/carbon cloth electrodes with two different morphol-

Received: April 6, 2013
Accepted: June 11, 2013
Published: June 11, 2013

   dx.doi.org/10.1021/am4012484 | ACS Appl. Mater. Interfaces 2013, 5, 6255−6260

ogies: (i) nanowire and (ii) nanosheet in order to investigate which nanostructure is the most favorable for capacitive energy storage applications. In addition, those hierarchical three-dimensional $NiCo_2O_4$ nanowires/nanosheets-carbon cloth electrodes could also be used in future applications such as electrode materials for Li/Na-ion batteries, electrocatalysts for oxygen evolution, electrosynthesis, and colloidal mediators for heat generator.

2. EXPERIMENTAL SECTION

2.1. Synthesis of the $NiCo_2O_4$ Nanowire and Nanosheet on Carbon Cloth. Prior to deposition, commercial carbon cloths (from Shanghai Liso New Material Technology Co., Ltd., Shanghai, P. R. of China) were cleaned by sonication sequentially in acetone, 1 M H_2SO_4 solution, deionized (DI) water, and ethanol for 15 min each. After being dried, the well-cleaned carbon cloth was transferred into Teflon-lined stainless autoclave. In a typical synthesis of $NiCo_2O_4$ nanowire, 1 mmol of $Ni(NO_3)_2{\cdot}6H_2O$, 2 mmol of $Co(NO_3)_2{\cdot}6H_2O$, 2 mmol of NH_4F, and 6 mmol o $CO(NH_2)_2$ were dissolved in 80 mL of mixed solution with ethanol and H_2O (V:V = 1:1) by constant intense stirring. The solution was then transferred into a Teflon-lined stainless autoclave and the pretreated carbon cloth (1 cm × 4 cm) was placed in the autoclave that was then sealed and maintained at 95 °C for 10 h. After the autoclave cooled to room temperature, the product was collected, washed, vacuum-dried, and then thermal treated at 350 °C in air atmosphere for 6 h. The mass of the $NiCo_2O_4$ nanowire deposited on carbon cloth was 0.52 mg/cm^2.

In the preparation of $NiCo_2O_4$ nanosheet, 1 mmol of $Ni(NO_3)_2{\cdot}6H_2O$, 2 mmol of $Co(NO_3)_2{\cdot}6H_2O$, and 1 g of hexadecyltrimethyl ammonium bromide were dissolved in 80 mL of mixed solution of methanol and H_2O (V:V = 5:1) by vigorous magnetic stirring. The resulting solution was then transferred into 100 mL Teflon-lined stainless steel autoclave. A piece of carbon cloth (1 cm × 4 cm) was immersed in the growing solution in the autoclave followed by heating the autoclave at 180 °C for 12 h. After the solution was cooled down to room temperature, the product was collected, washed, vacuum-dried and then thermal treated at 350 °C in air atmosphere for 6 h. The mass $NiCo_2O_4$ nanosheet deposited on carbon cloth was 0.6 mg/cm^2.

2.2. Materials Characterization. The products were characterized by field emission scanning electron microscopy (FESEM; S-4800, Japan) and transmission electron microscope (TEM; JEM-2010, Japan). Nitrogen adsorption/desorption isotherms were measured at the liquid nitrogen temperature using a Micromeritics Tristar 3000 analyzer.

2.3. Electrochemical Measurement. The $NiCo_2O_4$/carbon cloth directly acted as the working electrode for the following electrochemical tests by cyclic voltammetry (CV) and galvanostatic charge–discharge performed with a CHI660D electrochemical working station. All measurements were carried out in a three-electrode cell with a working electrode, a platinum plate counter electrode and a saturated calomel electrode (SCE) as the reference electrode at room temperature. The electrolyte was a 1 M KOH aqueous solution.

3. RESULTS AND DISCUSSION

3.1. Synthesis of the $NiCo_2O_4$ Nanowire and Nanosheet/Carbon Cloth. Two steps are involved in the synthesis strategy, which are a hydrothermal process of mixed metal precursors (Ni, Co) and subsequently a calcination process in air atmosphere. The $NiCo_2O_4$ nanowire results from thermal decomposition of basic metal (Ni, Co) carbonate hydroxide nanowire. The reactions involved may be illustrated as follows.[31−33]

$$Ni^{2+} + 2Co^{2+} + 3xF^- \rightarrow [NiCo_2F_{3x}]^{3(x-2)-} \quad (1)$$

$$CO(NH_2)_2 + H_2O \rightarrow 2NH_3 + CO_2 \quad (2)$$

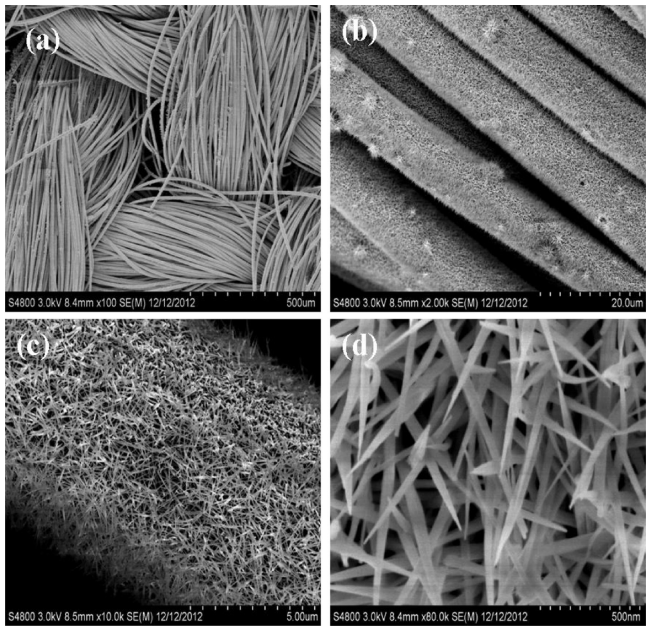

Figure 1. (a–d) FESEM images of the $NiCo_2O_4$ nanowire growing on carbon cloth at different magnifications.

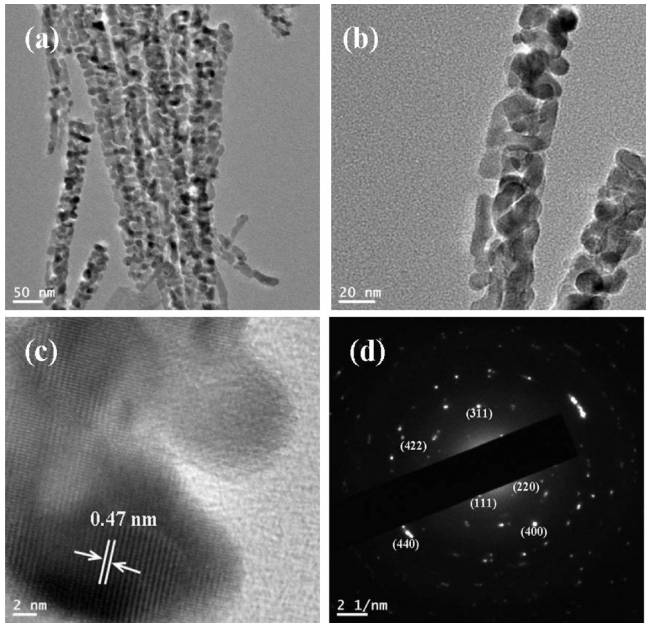

Figure 2. (a, b) TEM images, (c) HRTEM images, and (d) the SAED pattern of hierarchical $NiCo_2O_4$ nanowires.

$$CO_2 + H_2O \rightarrow CO_3^{2-} + 2H^+ \quad (3)$$

$$NH_3{\cdot}H_2O \rightarrow NH_4^+ + OH^- \quad (4)$$

$$[NiCo_2F_{3x}]^{3(x-2)-} + 1.5(2-y)CO_3^{2-} + 3yOH^- + nH_2O \rightarrow NiCo_2(OH)_{3y}(CO_3)_{1.5(2-y)}{\cdot}nH_2O + 3xF^- \quad (5)$$

$$2NiCo_2(OH)_{3y}(CO_3)_{1.5(2-y)}{\cdot}nH_2O + O_2 \rightarrow 2NiCo_2O_4 + (3y+2n)H_2O + 3(2-y)CO_2 \quad (6)$$

dx.doi.org/10.1021/am4012484 | ACS Appl. Mater. Interfaces 2013, 5, 6255−6260

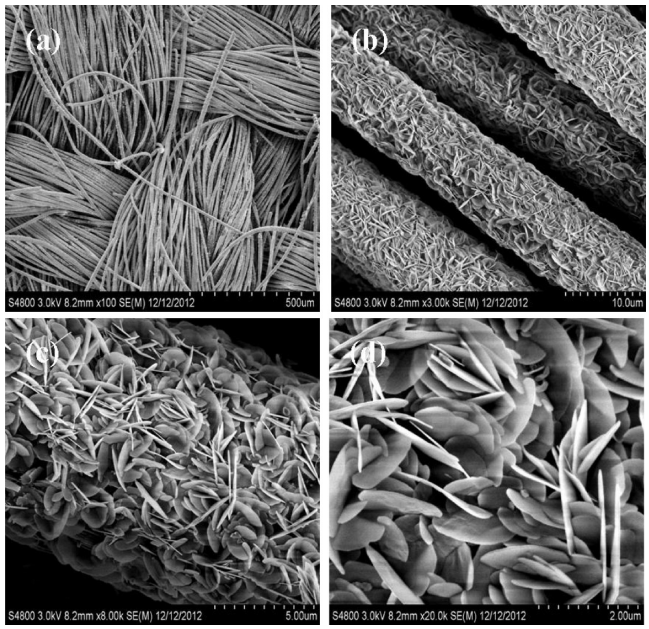

Figure 3. (a–d) FESEM images of the $NiCo_2O_4$ nanosheet growing on carbon cloth at different magnifications.

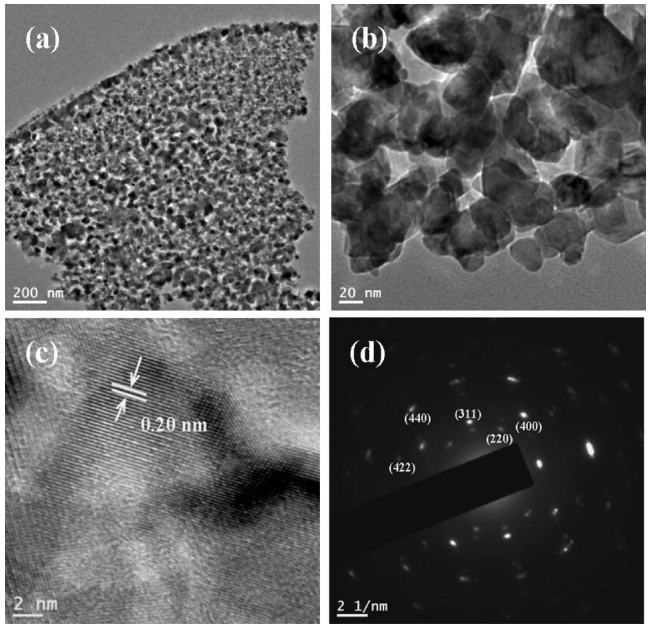

Figure 4. (a, b) TEM images, (c) HRTEM images, and (d) the SAED pattern of hierarchical $NiCo_2O_4$ nanosheets.

The formation process of $NiCo_2O_4$ nanosheet probably proceeds through the following reactions[23]

$$CH_3OH + H_2O \rightarrow CH_3OH_2^+ + OH^- \quad (7)$$

$$xNi^{2+} + 2xCo^{2+} + 6xOH^- \rightarrow Ni_xCo_{2x}(OH)_{6x} \quad (8)$$

$$2Ni_xCo_{2x}(OH)_{6x} + xO_2 \rightarrow 2xNiCo_2O_4 + 6xH_2O \quad (9)$$

3.2. Materials Characterization. The surface morphology of as-synthesized hierarchical $NiCo_2O_4$/carbon cloth is characterized by FESEM. Figure 1 shows low- and high-magnification FESEM images of the $NiCo_2O_4$ nanowire/carbon cloth. It is observed that $NiCo_2O_4$ nanowires with high density

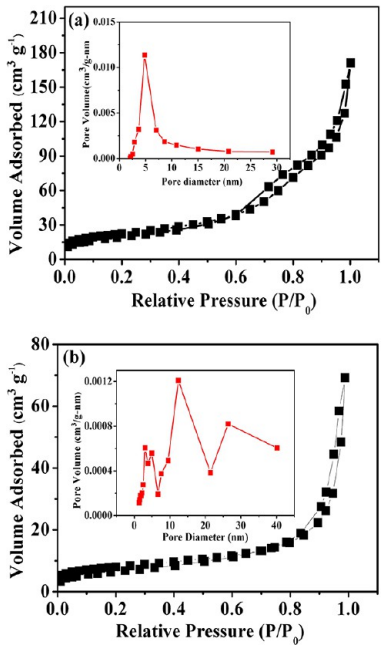

Figure 5. Nitrogen adsorption and desorption isotherms measured at 77 K for the hierarchical $NiCo_2O_4$ (a) nanowires and (b) nanosheets. The insets show the corresponding BJH pore size distributions.

are grown uniformly on carbon cloth, forming a 3D hierarchical structure (Figure 1a). The final product still keeps the ordered woven structure of the carbon cloth substrate. Meanwhile, carbon cloth can be readily rolled up, which is appropriate for flexible device applications. Higher-magnification FESEM images (Figure 1b–d) provide clearer information about the carbon cloth growing $NiCo_2O_4$ nanowires. As shown in Figure 1b, every $NiCo_2O_4$ nanowire/carbon fiber has uniform diameter of approximately 12 μm, which is slightly larger than that of pristine fiber diameter (ca. 9 μm) (not shown here). Further observation indicates that $NiCo_2O_4$ nanowires with sharp tips almost all grow vertically (Figure 1c, d). Furthermore the $NiCo_2O_4$ nanowire/carbon cloth has been ultrasonicated for several minutes before the FESEM examination, which confirms that the nanowires have a good adhesion on carbon cloth.

To further characterize the structure of the $NiCo_2O_4$ nanowire/carbon cloth, we carried out TEM studies (Figure 2). Figure 2a, b displays typical TEM images of nanowires scraped off from carbon cloth. We can clearly see that the diameters of the nanowires vary from nearly 10 to 40 nm from the point of contact to carbon cloth to the tip with many mesopores widely distributed on the surface. The lattice spacing of 0.47 nm corresponds to the (111) crystal plane of spinel $NiCo_2O_4$, as seen from the HRTEM image (Figure 2c). The selected area of electron diffraction (SAED) pattern (Figure 2d) demonstrates a polycrystalline structure of the $NiCo_2O_4$ nanowire. All the rings in SAED in Figure 2d recorded from the nanowires in Figure 1c can be uniquely indexed by the spinel $NiCo_2O_4$ crystal structure (JCPDS No. 20–0781, $a = b = c = 0.811$ nm).

The microstructure of $NiCo_2O_4$ nanosheet/carbon cloth is also investigated by FESEM and TEM. Figure 3 displays the FESEM images of $NiCo_2O_4$ nanosheet/carbon cloth at different magnifications. From low magnification FESEM image (Figure 3a), the carbon cloth depositing $NiCo_2O_4$

dx.doi.org/10.1021/am4012484 | ACS Appl. Mater. Interfaces 2013, 5, 6255–6260

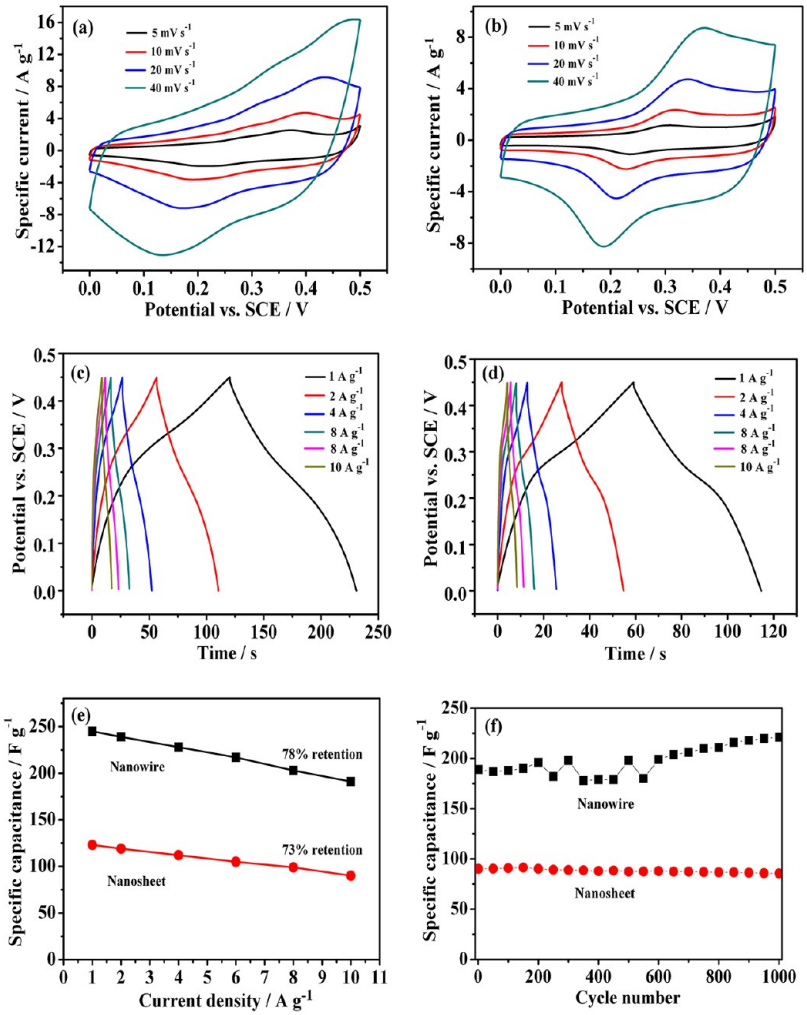

Figure 6. (a, b) CV curves, (c, d) charge–discharge curves, (e) capacitances versus current densities, and (f) variation of capacitance with cycle number at 10 A g^{-1} of the (a, c) $NiCo_2O_4$ nanowires/carbon cloth and the (b, d) $NiCo_2O_4$ nanosheet/carbon cloth.

nanosheets is still woven by carbon fibers. Each carbon fiber is uniformly covered by $NiCo_2O_4$ nanosheets (Figure 3b). Further observation indicates that these nanosheets are grown vertically and cross-linked on the carbon fiber (Figure 3c, d). From TEM images (Figure 4a, b), $NiCo_2O_4$ nanoparticles (ca. 20 nm) are arranged randomly to form the nanosheet structures, which confirms the mesoporous nature of $NiCo_2O_4$ nanosheets. The lattice resolved HRTEM image of a part of one $NiCo_2O_4$ nanocrystal is shown in Figure 4c. The interplanar spacing is measured to be 0.20 nm, corresponding to the (400) crystal plane. SAED performed on the region in Figure 4c is shown in Figure 4d. The diffraction rings can be indexed to the $NiCo_2O_4$ crystal structure (JCPDS No. 20–0781, $a = b = c = 0.811$ nm).

The nitrogen adsorption and desorption isotherms of the $NiCo_2O_4$ nanowires and nanosheets are shown in Figure 5. The Brunauer–Emmett–Teller (BET) surface area value of the nanowire and nanosheet is calculated to be 79.34 and 28.22 m^2 g^{-1}, respectively. Distinct hysteresis loop can be observed in the range of 0.7–1.0 P/P_o (Figure 5a, b), which suggests the presence of a mesoporous structure for the nanowires and nanosheets.[34−36] The pore size distribution of the sample calculated by desorption isotherm using Barret–Joyner–Halenda (BJH) method is shown in inset of Figure 5. The $NiCo_2O_4$ nanowires show narrow and ordered distributions of pores at ~4.86 nm (Figure 5a). The pore volume of nanowires is up to 0.26 cm^3 g^{-1}. The $NiCo_2O_4$ nanosheets have sharp peaks at ~3.04, 4.97, 12.46, and 26.44 nm (Figure 5b). The pore volume of nanosheets is calculated as 0.11 cm^3 g^{-1}. In consideration of high surface area, large pore volume, and ordered pore distribution, it is expected that the nanowires will have impressive electrochemical performance, and further characterizations have been carried out to prove this hypothesis.

3.3. Electrochemical Measurements. The transportation of electrolytes through the $NiCo_2O_4$/carbon cloth is feasible for efficient redox reactions during Faradaic charge storage process because of the mesoporosity and the hierarchical structure. However, the charge storage efficiency of the two microstructures may vary because of the observed differences in the morphology and size. To evaluate the properties of the prepared samples as supercapacitor electrodes, we perform cyclic voltammetry (CV) and galvanostatic charge–discharge measurements. Representative CV curves for the nanowire and nanosheet morphologies in three electrode configuration at different scan rates are shown in Figure 6a, b. As compared with CV curves of the $NiCo_2O_4$ nanowire, the $NiCo_2O_4$ nanosheet has more distinct redox peaks. However, the area under the CV curve is clearly much larger for the nanowire than for the nanosheet at the same scan rate. It is well-known that the

specific capacitance is proportional to the area of the CV curve.[37,38] This shows that the $NiCo_2O_4$ nanowire has higher capacitances than that of the $NiCo_2O_4$ nanosheet. The redox peaks correspond to the conversion between different cobalt and nickel oxidation states. The most plausible elementary processes associated with the capacitive behavior of $NiCo_2O_4$ can be described as follows[39,40]

$$NiCo_2O_4 + OH^- + H_2O \leftrightarrow NiOOH + 2CoOOH + e^- \quad (10)$$

$$CoOOH + OH^- \leftrightarrow CoO_2 + H_2O + e^- \quad (11)$$

Galvanostatic charge−discharge is a complementary method for measuring the specific capacitance of electrochemical capacitors at constant current. Panels c and d in Figure 6 show galvanostatic charge−discharge curves of the $NiCo_2O_4$ nanowire and nanosheets at various current densities. The increase in the charging time represents the higher capacitance of the nanowire. The specific capacitance can be calculated by $It/(Vm)$, where I is the discharging current, t is the discharging time, V is the potential drop during discharge, and m is the mass of active material in a single electrode. The specific capacitance is shown as a function of the current density in Figure 6e. The specific capacitance of the $NiCo_2O_4$ nanowire is 245, 239, 228, 217, 203, and 191 F g^{-1} at 1, 2, 4, 6, 8, and 10 A g^{-1} current density, respectively. In contrast, the specific capacitance of the $NiCo_2O_4$ nanowire is 123, 119, 112, 105, 99, and 90 F g^{-1} at 1, 2, 4, 6, 8, and 10 A g^{-1}, respectively. This is in agreement with the result of the CV curves. In addition, the capacitance retention from 1 to 10 A g^{-1} is also better for nanowire (78%) than for nanosheet (73%).

Because a long cycling performance is among the most important criteria for a supercapacitor,[41,42] an endurance test is conducted using galvanostatic charge−discharge cycles at 10 A g^{-1} (Figure 6f). The specific capacitance of the $NiCo_2O_4$ nanowire increases with cycling numbers, instead of decreasing as in most cycle tests. After a 1000-cycle test, the specific capacitance reaches a high value of 221 F g^{-1}, which is higher than its initial value (190 F g^{-1}). As for the $NiCo_2O_4$ nanosheet, the decay in specific capacitance after a 1000-cycle test is 5% (Figure 6f). These results indicate that the $NiCo_2O_4$ nanowire has a better cycling performance in comparison with the $NiCo_2O_4$ nanosheet.

Taking specific capacitance, rate capability, and cycling performance into account, the $NiCo_2O_4$ nanowire shows higher capacitive behaviors than the $NiCo_2O_4$ nanosheet in our system. We postulate that two factors endow the $NiCo_2O_4$ nanowire with superior electrochemical performance. First, larger surface area and larger pore volume endow the nanowire with more electron/ion paths for feasible ion transport and fast redox reaction. Second, from the CV curves (Figure 6a, b), the higher capacitance for the $NiCo_2O_4$ nanowires may be due to the combination of Faradic and electrical double-layer capacitances.

4. CONCLUSIONS

In summary, mesoporous $NiCo_2O_4$ nanowires and nanosheets are successfully grown on carbon cloth through a facile two-step method. Each nanowire or nanosheet renders direct contact with the carbon fiber and creates unique supercapacitor electrodes. In view of the difference of surface area and pore volume, the two crystals present different pseudocapacitive performance. The $NiCo_2O_4$ nanowires/carbon cloth shows higher supercapacitor performance than that of the $NiCo_2O_4$ nanosheets/carbon cloth. This comparison through different morphology offers strategies to enhance the performance of supercapacitor electrodes. More importantly, the as-synthesized hierarchical $NiCo_2O_4$ nanocrystal/carbon cloth could be applied in alternative energy generation and storage devices.

AUTHOR INFORMATION

Corresponding Author

*E-mail: xfwang@tongji.edu.cn.

Notes

The authors declare no competing financial interest.

ACKNOWLEDGMENTS

The authors gratefully acknowledge the financial support offered by NSFC Grant (21173158) and STCSM (10PJ1409600).

REFERENCES

(1) Sharma, Y.; Sharma, N.; Subba Rao, G. V.; Chowdari, B. V. R. *Adv. Funct. Mater.* **2007**, *17*, 2855−2861.
(2) Wang, Q.; Liu, B.; Wang, X.; Ran, S.; Wang, L.; Chen, D.; Shen, G. *J. Mater. Chem.* **2012**, *22*, 21647−21653.
(3) Zhu, J.; Gao, Q. *Microporous Mesoporous Mater.* **2009**, *124*, 144−152.
(4) Liang, Y.; Wang, H.; Zhou, J.; Li, Y.; Wang, J.; Regier, T. Z.; Dai, H. *J. Am. Chem. Soc.* **2012**, *134*, 3517−3523.
(5) Wang, H.; Yang, Y.; Liang, Y.; Zheng, G.; Li, Y.; Cui, Y.; Dai, H. *Energy Environ. Sci.* **2012**, *5*, 7931−7935.
(6) Wang, H.; Gao, Q.; Jiang, L. *Small* **2011**, *7*, 2454−2459.
(7) wei, T. Y.; Chen, C. H.; Chien, H. C.; Lu, S. Y.; Hu, C. C. *Adv. Mater.* **2010**, *22*, 347−351.
(8) Ding, R.; Qi, L.; Wang, H. *J Solid State Electrochem.* **2012**, *16*, 3621−3633.
(9) Chang, S. K.; Lee, K. T.; Zainal, Z.; Tan, K. B.; Yusof, N. A.; Yusoff, W. M. D. W.; Lee, J. F.; Wu, N. L. *Electrochim. Acta* **2012**, *67*, 67−72.
(10) Wang, H. W.; Hu, Z. A.; Chang, Y. Q.; Chen, Y. L.; Wu, H. Y.; Zhang, Z. Y.; Yang, Y. Y. *J. Mater. Chem.* **2011**, *21*, 10504−10511.
(11) Yuan, C.; Li, J.; Hou, L.; Yang, L.; Shen, L.; Zhang, X. *J. Mater. Chem.* **2012**, *22*, 16084−16090.
(12) Jiang, H.; Ma, J.; Li, C. *Chem. Commun.* **2012**, *48*, 4465−4467.
(13) Lu, Q.; Chen, Y.; Li, W.; Chen, J. G.; Xiao, J. Q.; Jiao, F. *J. Mater. Chem. A* **2013**, *1*, 2331−2336.
(14) Wu, T.; Li, J.; Hou, L.; Yuan, C.; Yang, L.; Zhang, X. *Electrochim. Acta* **2012**, *81*, 172−178.
(15) Xiao, J.; Yang, S. *RSC Adv.* **2011**, *1*, 588−595.
(16) Chien, H. C.; Cheng, W. Y.; Wang, Y. H.; Lu, S. Y. *Adv. Funct. Mater.* **2012**, *22*, 5038−5043.
(17) Zhang, G. Q.; Wu, H. B.; Hoster, H. E.; Chan−Park, M. B.; Lou, X. W. *Energy Environ. Sci.* **2012**, *5*, 9453−9456.
(18) Wang, Q.; Wang, X.; Liu, B.; Yu, G.; Hou, X.; Chen, D.; Shen, G. *J. Mater. Chem. A* **2013**, *1*, 2468−2473.
(19) Yuan, C.; Li, J.; Hou, L.; Zhang, X.; Shen, L.; Lou, X. W. *Adv. Funct. Mater.* **2012**, *22*, 4592−4597.
(20) Zhang, G.; Lou, X. W. *Adv. Mater.* **2013**, *25*, 976−979.
(21) Xing, W.; Qiao, S. Z.; Wu, X. Z.; Gao, X. L.; Zhou, J.; Zhuo, S. P.; Hartono, S. B.; Hulicova−Jurcakova, D. *J. Power Sources* **2011**, *196*, 4123−4127.
(22) Grdeń, M.; Alsabet, M.; Jerkiewicz, G. *ACS Appl. Mater. Interfaces* **2012**, *4*, 3012−3021.
(23) Rakhi, R. B.; Chen, W.; Cha, D.; Alshareef, H. N. *Nano Lett.* **2012**, *12*, 2559−2567.
(24) Gupta, V.; Gupta, S.; Miura, N. *J. Power Sources* **2010**, *195*, 3757−3760.
(25) Bao, L.; Zang, J.; Li, X. *Nano Lett.* **2011**, *11*, 1215−1220.

(26) Zhang, X.; Gong, L.; Liu, K.; Cao, Y.; Xiao, X.; Sun, W.; Hu, X.; Gao, Y.; Chen, J.; Zhou, J.; Wang, Z. L. *Adv. Mater.* **2010**, *22*, 5292−5296.
(27) Liu, B.; Zhang, J.; Wang, X.; Chen, G.; Chen, D.; Zhou, C.; Shen, G. *Nano Lett.* **2012**, *12*, 3005−3011.
(28) Wang, Z.; Wang, H.; Liu, B.; Qiu, W.; Zhang, J.; Ran, S.; Huang, H.; Xu, J.; Han, H.; Chen, D.; Shen, G. *ACS Nano* **2011**, *5*, 8412−8419.
(29) Liu, B.; Wang, Z.; Dong, Y.; Zhu, Y.; Gong, Y.; Ran, S.; Liu, Z.; Xu, J.; Xie, Z.; Chen, D.; Shen, G. *J. Mater. Chem.* **2012**, *22*, 9379−9384.
(30) Yang, L.; Cheng, S.; Ding, Y.; Zhu, X.; Wang, Z. L.; Liu, M. *Nano Lett.* **2012**, *12*, 321−325.
(31) Jiang, J.; Liu, J. P.; Huang, X. T.; Li, Y. Y.; Ding, R. M.; Ji, X. X.; Hu, Y. Y.; Chi, Q. B.; Zhu, Z. H. *Cryst. Growth Des.* **2010**, *10*, 70−75.
(32) Liu, J.; Jiang, J.; Cheng, C.; Li, H.; Zhang, J.; Gong, H.; Fan, H. J. *Adv. Mater.* **2011**, *23*, 2076−2081.
(33) Xia, X.; Tu, J.; Zhang, Y.; Wang, X.; Gu, C.; Zhao, X. B.; Fan, H. J. *ACS Nano* **2012**, *6*, 5531−5538.
(34) Tao, Y. S.; Kanoh, H.; Abrams, L.; Kaneko, K. *Chem. Rev.* **2006**, *106*, 896−910.
(35) Wang, H. L.; Gao, Q. M.; Jiang, L. *Small* **2011**, *7*, 2454−2459.
(36) Yu, J. G.; Wang, G. H.; Cheng, B.; Zhou, M. H. *Appl. Catal., B* **2007**, *69*, 171−180.
(37) Lee, J. W.; Hall, A. S.; Kim, J. D.; Mallouk, T. E. *Chem. Mater.* **2012**, *24*, 1158−1164.
(38) Wang, H. W.; Hu, Z. A.; Chang, Y. Q.; Chen, Y. L.; Zhang, Z. Y.; Yang, Y. Y.; Wu, H. Y. *Mater. Chem. Phys.* **2011**, *130*, 672−679.
(39) Wang, X.; Han, X.; Lim, M.; Singh, N.; Gan, C. L.; Ma, J.; Lee, P. S. *J. Phys. Chem. C* **2012**, *116*, 12448−12454.
(40) Wu, Y. P.; Wang, F.; Xiao, S.; Hou, Y.; Hu, C. L.; Liu, L. *RSC Adv.* **2013**, DOI: 10.1039/C3RA23466E.
(41) Wang, H.; Casalongue, H. S.; Liang, Y.; Dai, H. *J. Am. Chem. Soc.* **2010**, *132*, 7472−7477.
(42) Wang, H.; Wang, Y.; Hu, Z.; Wang, X. *ACS Appl. Mater. Interfaces* **2012**, *4*, 6827−6834.